



Aerogravity and remote sensing observations of an iron deposit in Gara Djebilet, southwestern Algeria



Mohand Bersi ^a, Hakim Saibi ^{b,*}, Moulley Charaf Chabou ^c

^a Department of Geophysics, Faculty of Earth Sciences, Geography and Territorial Planning, Houari Boumediene University of Sciences and Technology, BP 32 Al Alia, 16111, Algiers, Algeria

^b Laboratory of Exploration Geophysics, Department of Earth Resources Engineering, Faculty of Engineering, Kyushu University, 744 Motooka, Nishi-ku, Fukuoka, 819-0395, Japan

^c Université Ferhat Abbas, Sétif 1, Institut d'Architecture et des Sciences de la Terre, Département des Sciences de la Terre, Campus El-Bez, 19000, Sétif, Algeria

ARTICLE INFO

Article history:

Received 12 June 2015

Received in revised form

17 December 2015

Accepted 4 January 2016

Available online 5 January 2016

Keywords:

Algeria

Remote sensing

Landsat 8

Gara Djebilet

Iron ore

Aerogravity

ABSTRACT

The Gara Djebilet iron ore region is one of the most important regions in Africa. Located in the southwestern part of Algeria at the border with Mauritania, the Gara Djebilet region is characterized by steep terrain, which makes this area not easily accessible. Due to these conditions, remote sensing techniques and geophysics are the best ways to map this iron ore. The Gara Djebilet formations are characterized by high iron content that is especially rich in hematite, chamosite and goethite. The high iron content causes an absorption band at 0.88 μm, which is referred to as band 5 in the Operational Land Imager (OLI) Landsat 8 images. In this study, we integrated geological data, aerogravity data, and remote sensing data for the purpose of mapping the distribution of the Gara Djebilet iron deposit.

Several remote sensing treatments were applied to the Landsat 8 OLI image, such as color composites, band ratioing, principal component analysis and a mathematical index, which helped locate the surface distribution of the iron ore. The results from gravity gradient interpretation techniques, 2-D forward modeling and 3-D inversion of aerogravity data provided information about the 2-D and 3-D distribution of the iron deposit. The combination of remote sensing and gravity results help us evaluate the ore potential of Gara Djebilet. The estimated tonnage of the iron ore at Gara Djebilet is approximately 2.37 billion tonnes with 57% Fe.

© 2016 Elsevier Ltd. All rights reserved.

1. Introduction

The iron industry in Algeria has expanded over the last 20 years; the demand for this resource is growing continuously. Algeria has two large deposits of iron, but only the ore of El Ouenza (NE Algeria, 60 million tonnes) is currently exploited. The deposit of oolitic iron at Gara Djebilet represents the largest deposit of iron in the country and in North Africa (1 billion tonnes of iron at a grade of 57% iron, Taib, 2009) but is in an isolated and hardly accessible area. Thus, it was not until the historic visit of the Algerian Prime Minister in July 2013 that mine operations at Gara Djebilet were launched to counter high market demand, especially to supply large Algerian national projects (East-West highway, Algiers Metro, infrastructure and housing projects).

The Gara Djebilet oolitic iron deposit is situated in the

southwest of the Tindouf Basin (Fig. 1) and was discovered by Gevin in 1952. The Gara Djebilet region is characterized by steep terrain, which makes this area not easily accessible (1600 km south of the Algerian Mediterranean coast) as it presents high topography (Fig. 2), and only one track of 200 km connects it with the city of Tindouf. Under such conditions, it is difficult to map accurately; the capacities of this deposit are still estimated by approximation.

Previous estimated of iron tonnage in Gara Djebilet are Matheron (1955): 2.65 billion tonnes (grade of 53–58% Fe); Guerrak (1988): 0.98 billion tonnes (grade of 57% Fe); Marelle and Abdulla (1970): 1.48 billion tonnes (grade of 49–54% Fe); The Ministry of Energy and Mining of Algeria (2005): 0.75 billion tonnes (grade of 58% Fe) (Porter GeoConsultancy, 2015). Ciampalini et al. (2013a,b) used Landsat ETM+ to visualize iron deposits in southwestern parts of Algeria.

Remote sensing techniques using multispectral images can recognize ore deposits (Sabins, 1999), and airborne gravity data analysis allows for detailed mapping of iron deposits. Many authors

* Corresponding author.

E-mail address: sabi-hakim@mine.kyushu-u.ac.jp (H. Saibi).

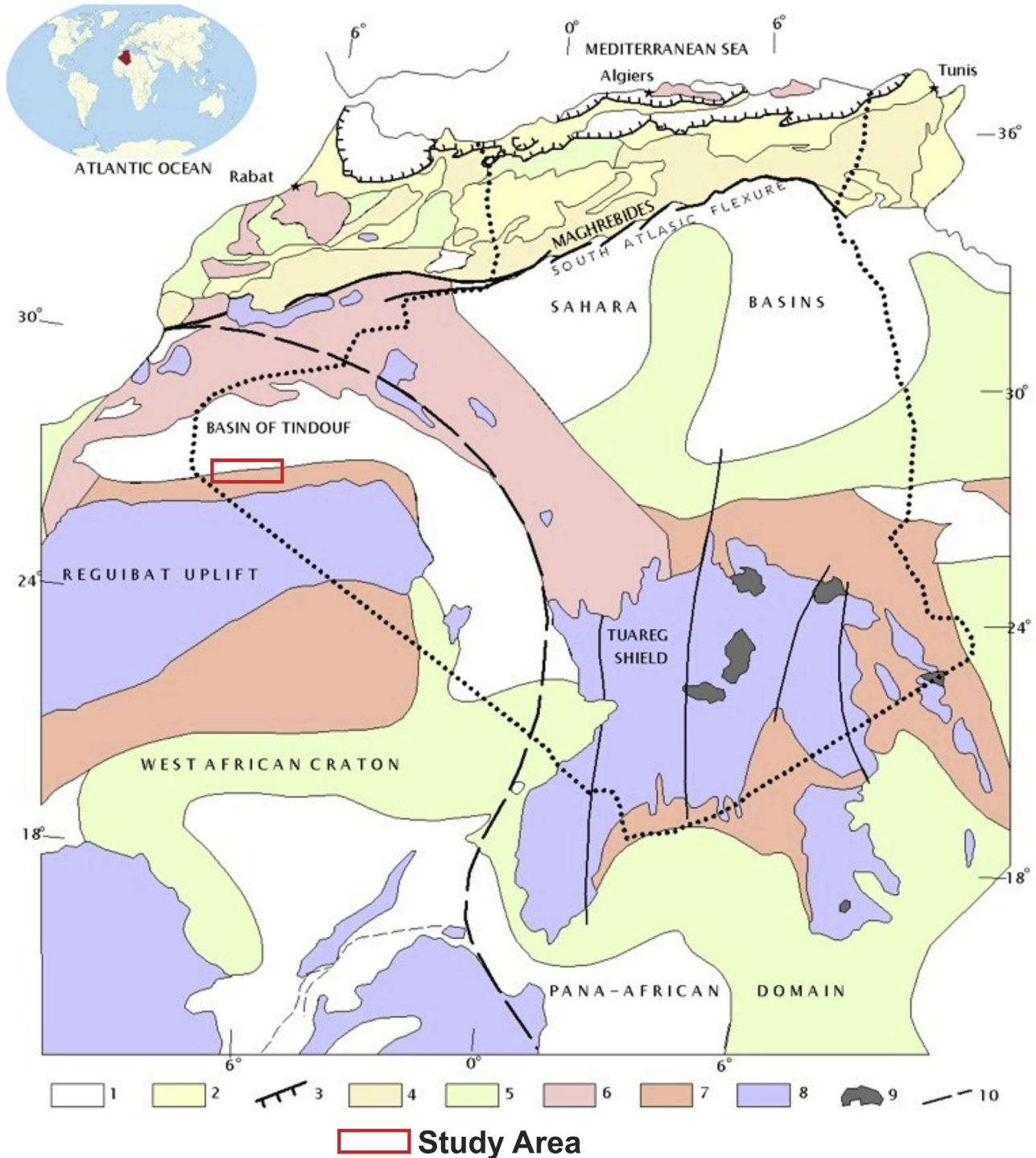


Fig. 1. Major geotectonic units of West Africa, modified from Fabre (1976). 1: Tertiary and Quaternary; 2: Alpine molasse; 3: Tertiary thrust sheet; 4: Secondary tabular; 5: Secondary plication; 6: Primary plication; 7: Primary tabular; 8: Precambrian and Early Cambrian Sahara; 9: Cenozoic magma; 10: Megafault. The study area is located in southwestern Algeria.

have used remote sensing techniques and geophysics separately or combined to map ores in general or iron ore specifically.

Hammer (1945) explained the application of Gauss's theorem to evaluate the mass of a causative body from gravity data. Seguin (1971) discovered iron ore by the gravity method in the central part of the Labrador Trough (Canada). Wang et al. (2012) inverted gravity data to explore mineral deposits in Henan Province (China). Martinez et al. (2013) inverted airborne gravity data for mineral exploration in Quadrilatero Ferrifero (Brazil). Dufrechou et al.

(2015) used gravity data to investigate mineralization in the Bandy gneiss complex (Greenville, Canada), and Woolrych et al. (2015) succeeded in the discovery of the Kitumba iron oxide copper gold deposit using airborne gravity data.

There are several examples of the application of remote sensing technologies in exploring iron ores. Murthy and Mallick (1984) applied Landsat MSS data to delineate the iron-ore-bearing zone in Goa (India). Abulghasem et al. (2011) integrated remote sensing data and magnetic data for iron ore investigation in the western

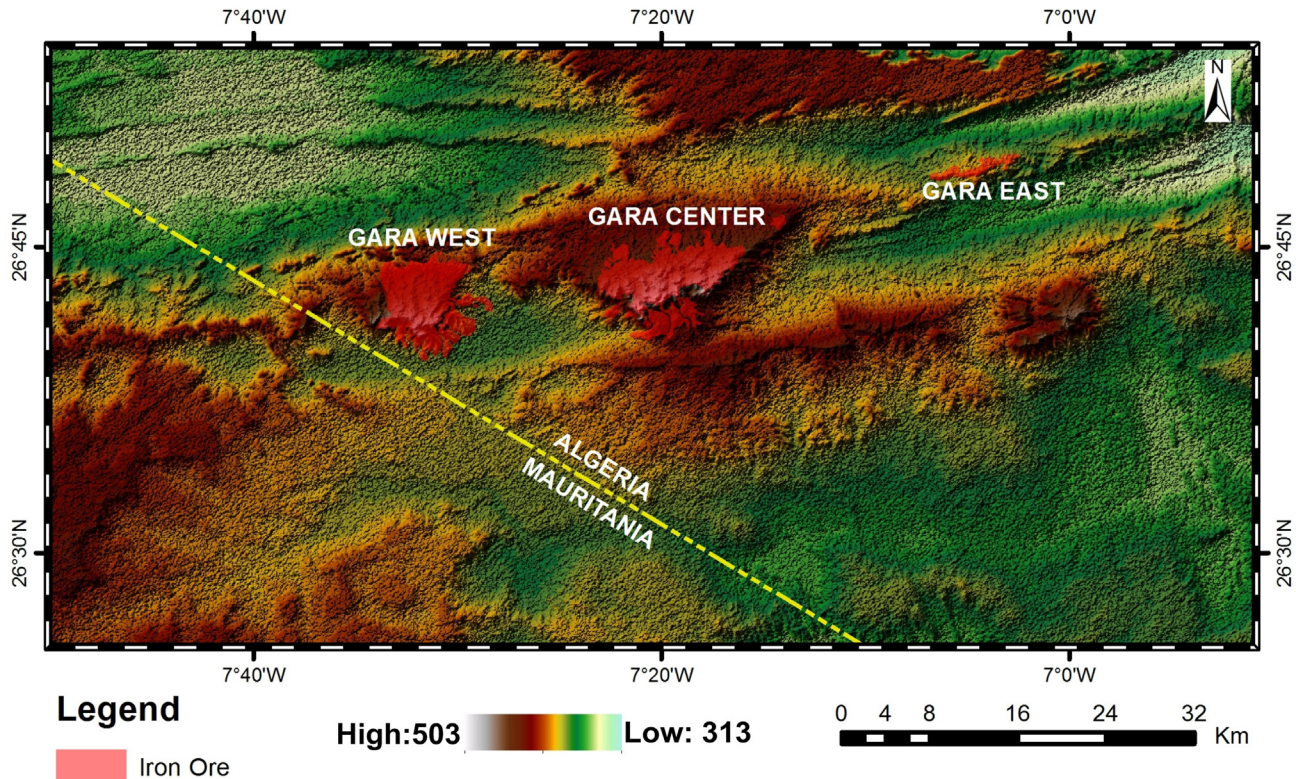


Fig. 2. Digital elevation model of the study area.

part of Wadi Shatti District (Libya). Mouton (2002) combined gravity data and remote sensing data (Landsat 5) to delineate a new iron ore deposit in northern Cape Province (South Africa). Feizi and Mansouri (2013) used ASTER and ETM7+ satellite images to study the iron potential of Qom Province (Iran).

The gravity method has a unique advantage for iron ore investigation as it responds directly to the density contrast between high-density iron ore and low-density surrounding rocks. Thus, deposits of high-density iron ore yield gravity highs. In addition, the gravity technique enables an estimation of the total mass responsible for such gravity anomaly.

The main objective of this study is to evaluate the potential of the Gara Djebilet iron ore using two different data sets, the first consisting of OLI Landsat 8 images and the second consisting of airborne gravity data.

The images from Landsat 8 of the Gara Djebilet area (Path/Row number 201/41) include this scene imaged on August 2, 2014 taken from the Landsat 8 satellite and acquired from <http://earthexplorer.usgs.gov>.

The airborne gravity data set consists of gravity data downloaded from <http://bgi.omp.obs-mip.fr> and provided by the BGI (International Gravimetric Office). These data were used to understand thickness and volume of the gravity source (iron ore) responsible for such high gravity anomalies.

Image processing techniques (color composites, band ratioing, principal component analysis and indexes) and gravity analysis (Bouguer anomaly, analytic signal, tilt derivative, 2-D modeling and 3-D inversions of gravity data) were used, and pertinent results were obtained. Remote sensing contributed to surface recognition of the iron ore distribution, and gravity analysis allowed us to detect the depth extent of the iron ore distribution and to estimate the total tonnage, which is approximately 2.37 billion tonnes (57% Fe).

2. Geological setting

The Gara Djebilet iron ore deposit is located in the southern flank of the Tindouf basin (Southwestern Algeria), and belongs to the North African Palaeozoic oolitic ironstone belt, extending more than 3000 km from Zemmour (Mauritania) to Libya, containing ironstones of Ordovician, Silurian and Devonian age (Guerrak, 1988, 1991).

The Tindouf basin is a large ($120,000 \text{ km}^2$) elongated WSW-ENE-trending syncline bordered by the basement of the Reguibat shield (Yetti-Eglab massif) in the South, the Anti-Atlas in the North, the Reggane basin and the Ougarta range in the east and the El Aioun basin and the Mauritanides belt in the west. On the southern flank of the Tindouf basin, the Paleoproterozoic basement (2.21–2.07 Ga) of the Yetti-Eglab massif (Peucat et al., 2005) is covered by up to 2000 m succession of Upper Ordovician to late Carboniferous rocks (Gevin, 1960; Guerrak, 1988; Bitam et al., 1996) (Figs. 3 and 4). The sedimentary succession begins with the Upper Ordovician glaciogenic sandstones (Gevin and Mongereau, 1968) of the "Ghezziane formation". It is followed by the Silurian shales of "Sebkha Mabbes formation". Early Devonian sediments, known as "Gara Djebilet formation", consist mostly of sandstone with shale intercalations. It is divided into two members: the lower "Grès de Djebilet" member of Lockhonian-Pragian age, and the upper "Grès supra-minéraux" member of Emsian age. Middle Devonian sediments (Oued Talha formation) are mainly composed of shales (lower "Oued Talha" member, Eifelian) and limestones (upper "Kerba Tsabia" member, Givetian). Upper Devonian (Kereb En Naga formation) comprises Frasnian siltstones (Oued Rhazzal member) and Famennian shales (Oued Slouguia member) which hosts the Mecheri Abdelaziz oolitic iron deposit, located 250 km in the East of Gara Djebilet (Guerrak and Chauvel, 1985). The Carboniferous comprises 4 formations: shales and limestones of Tournaisian (Kreb

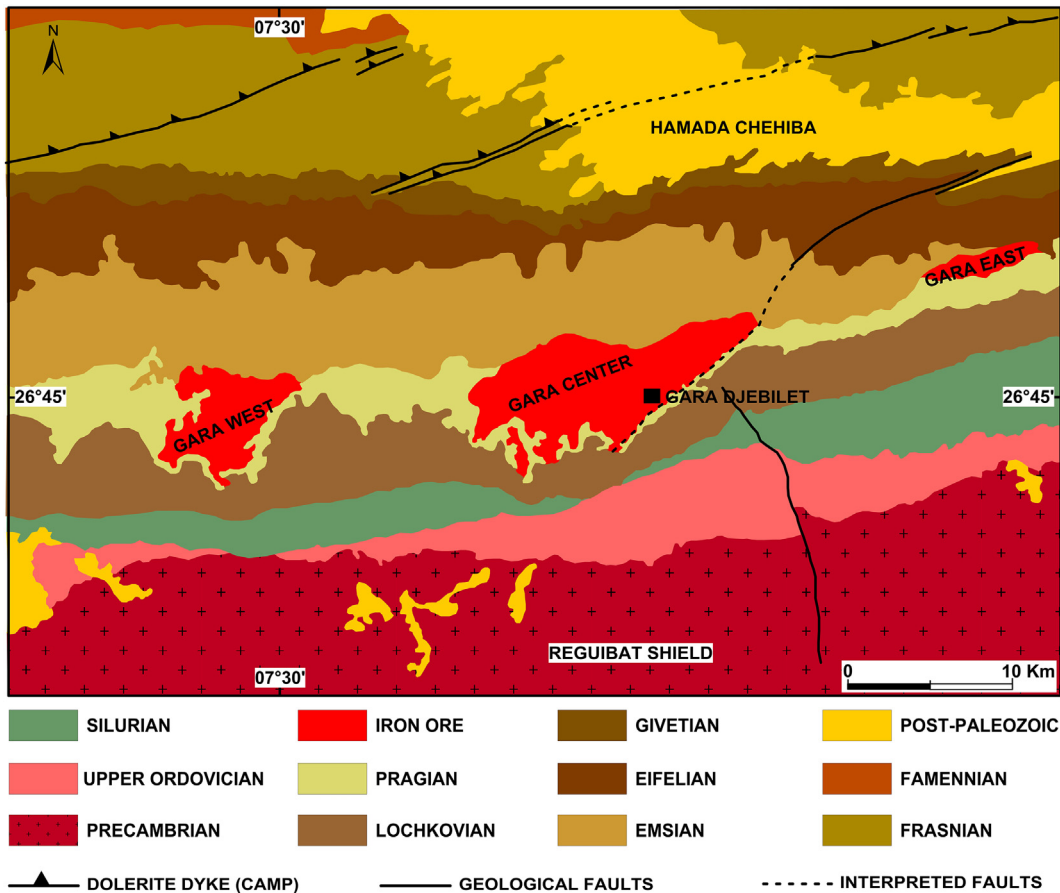


Fig. 3. Geologic map of the Djebilet area.

es Slouguia formation), lower Visean (Kreb es Sefiat formation) and upper Visean (Ain el Barka formation) age; finally, the succession ends with shales, sandy shales and sandstones of Namurian and Westphalian age (Hassi Aoulouel formation).

A few isolated long dolerite dykes, WSW-ENE trending, crosscut the entire Paleozoic terrains of the area, and are part of the ~201 Ma Central Atlantic Magmatic Province (CAMP) (Chabou et al., 2007, 2010). These dykes are probably responsible of the metamorphism of the Gara Djebilet oolitic iron ore (Fabre, 2005). In some area, dolerite sills of the CAMP intruded the Upper Devonian, and the few exploration wells drilled in the southern limb of Tindouf basin have also found dolerites lying directly on the basement or interbedded with the Upper Ordovician sandstones (Chabou et al., 2007).

The Cenozoic in the study area is represented by the Hamada of Kereb Cheheiba and the Quaternary by the large sand dunes of the "Erg Igoudi".

The chronological deposits of these formations can be synthesized by a stratigraphical column (Fig. 4).

3. Iron ore deposits of Gara Djebilet

The oolitic iron ore of Gara Djebilet is interbedded within the Early Devonian sediments (Gara Djebilet Formation), located at the lower and upper members boundary, between Pragian argillaceous sandstones of Lower "Grès de Djebilet" and Emsian conglomerates/sandstones of the Upper "Grès supra-minéraux" (Guerrak, 1988). Three main separate deposits were recognized throughout the area: Gara West (14 km length, 4 km width, 30 m thick), Gara

Center (20 km length, 5 km width, 30 m thick) and Gara East (7 km length, 1 km width, 9 m thick) extending West-East for about 60 km (Guerrak, 1988) (Fig. 3). The deposits are preserved as mesas of flat lying (1.5–2° north dipping) oolitic ironstone lenses interbedded with predominantly argillaceous and sandy sediments. According to Guerrak (1988), the main iron ore body can be subdivided into three zones: (1) the Lower non-magnetic ore (3–10 m thick, Fe = 54.6%), containing chamosite, siderite, hematite, goethite, apatite, quartz; (2) the Magnetic ore (6–10 m thick, Fe = 57.8%), which corresponds to the main economic ore, contains magnetite, maghemite, chamosite, siderite, hematite and apatite; and (3) the Upper non-magnetic ore (4–12 m thick, Fe = 53%) with goethite, chamosite, hematite, siderite, and apatite.

4. Remote sensing analysis

The Landsat 8 image covering the area of Gara Djebilet was calibrated and resized to the zone of interest. A series of grayscale visualizations were performed on the 6 bands (2, 3, 4, 5, 6 and 7) to obtain the reflectance values and the tint of the iron formations in all bands. This operation allows us to choose the best ratios and to define the iron ore index.

Band Sharpening is a technique that combines highly resolved, panchromatic data with low resolution, multispectral data. This fusion creates a product with the spectral characteristics of the multispectral data, while maintaining the spatial resolution of the panchromatic image (Vrabel, 1996). We employ the Color Normalized (CN) spectral sharpening technique to create the multispectral data with high spatial resolution, which has been

AGE	FORMATION	THICKNESS (m)	LITHOLOGY	
NAMURO-WESTPHALIAN	HASSI AOULEOUEL	350	SANDY SHALES, FINE SANDSTONES SHALES	
VISEAN	AIN EL BARKA	600	SHALES, LIMESTONES AND DOLOMITES	
			ANHYDRITE	
			SHALES AND LIMESTONES	
	KERB ES SEFIAT	310	SHALES AND LIMESTONES	
TOURNAISIAN	KERB ES SLOUGUIA	80-160	SHALES AND LIMESTONES	
FAMMENIAN	KERB EN NAGA	100-140	SILTSTONES AND SHALES	
	OUED GHAZAL	100-150	ARGILLACEOUS SILTSTONES	
FRASNIAN	OUED TSABIA	80-160	SHALES SILTSTONES AND LIMESTONES	
GIVETIAN	OUED TALHA	40-100	LIMESTONES AND SHALES	
EIFELIAN				
EMSIAN				
PRAGIAN	DJEBILET	50-100	SILTSTONES AND SANDSTONES	
LOCHKOVIAN				
SILURIAN	SEBKHA MABBES	80-200	SHALES	
CAMBRO-ORDOVICIAN	GHEZZIANE	0-70	SANDSTONE	
PRECAMBRIAN	YETTI-EGLAB	-	GRANITE	

Fig. 4. Synthetic stratigraphical column of Gara Djebilet (modified from Guerrak, 1988).

demonstrated to be effective in previous work (Vrabel et al., 2002).

The OLI panchromatic band (0.50–0.68 μm) has been used to sharpen the resolution of the 6 bands (Roy et al., 2014). The sharpened bands are used to make a natural light color composite corresponding to bands 4, 3 and 2 displayed in RGB mode. The composite of bands 6, 5 and 4 obtained from sharpened bands was

used to enhance the visualization of iron high-content zones. The iron ore presented a high content of iron, especially the hematite (Guerrak, 1988); it caused high absorption in the near infrared channel and in the far infrared channel (Clénet et al., 2010), corresponding, respectively, to band 5 and band 6 in the Landsat 8 sensor (Roy et al., 2014).

Ratioing is a processing technique where reflectance values in one channel are divided by values for the same pixel in another channel (Prost, 2014). The 4/5, 5/6 and 6/7 ratios are used to differentiate between the iron ore and the neighborhood formations. These three ratios initially have a 30-m resolution, but using the sharpening operation by the panchromatic band (band 8), the resolution is improved to 15 m. Principal component analysis (PCA) is used to reduce the number of initial data by eliminating redundancies. It allows for linear transformations of a large number of inter-correlated variables to obtain a limited number of uncorrelated components (Vogt and Tacke, 2001). This transformation provides a reduced number of channels while maintaining the maximum amount of information (Dronova et al., 2015). Investigation into the correlation coefficients displayed as radar shows that the PC4 component is the most correlated with the other bands (Fig. 5); this component will be used for display with the ENVI color table.

4.1. Color composites

The natural light composite (Fig. 6) shows the iron ore with a dark shade, which is due to the absorption of the electromagnetic

radiation in this range by the high ferric iron content. Two different zones can be observed in the iron ore area. The first is highlighted in dark red and corresponds to low iron content. The second is highlighted in dark blue and corresponds to high iron content. The false color composite of B6, 5 and 4, displayed in RGB mode and sharpened with the panchromatic band, shows the boundaries between the iron ore and the Paleozoic formations (Fig. 7). The iron ore is well highlighted, appearing in a dark blue color. The Devonian formation appears in red.

4.2. Band ratioing

The ratioing process depends on the spectral response of the different land classes in the 6 OLI multispectral bands. The most important differentiation between the iron ore and the surrounding formations is observed in the range between band 4 and band 7 (0.66–2.29 μm). The ratios 4/5, 5/6 and 6/7 were chosen, respectively, for an RGB display (Fig. 8).

In band 4 (0.64–0.67 μm), the iron formations absorb little, unlike in bands 5 and 7, where the iron formations readily absorb more electromagnetic radiation than the surrounding formations (Fig. 9). The 4/5 ratio presents high values for the iron ore (near 1),

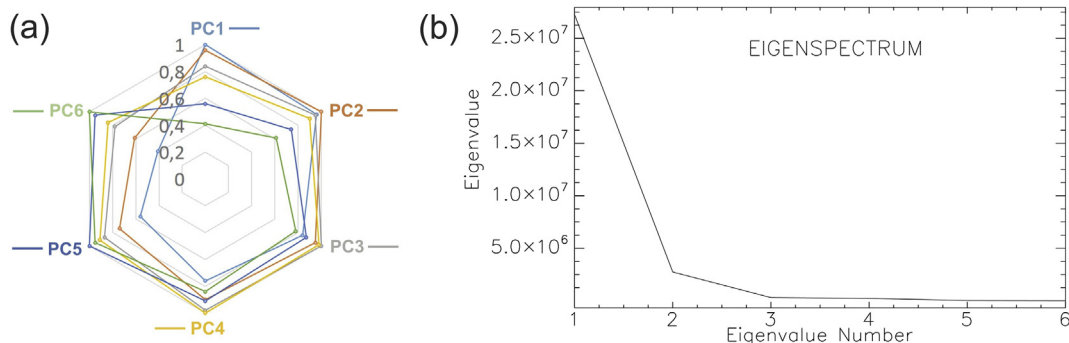


Fig. 5. (a) Radar showing correlation coefficients. PC4 is the most correlated with the other PCs. (b) Eigenvalues spectrum showing the maximum information contained in the first three components.

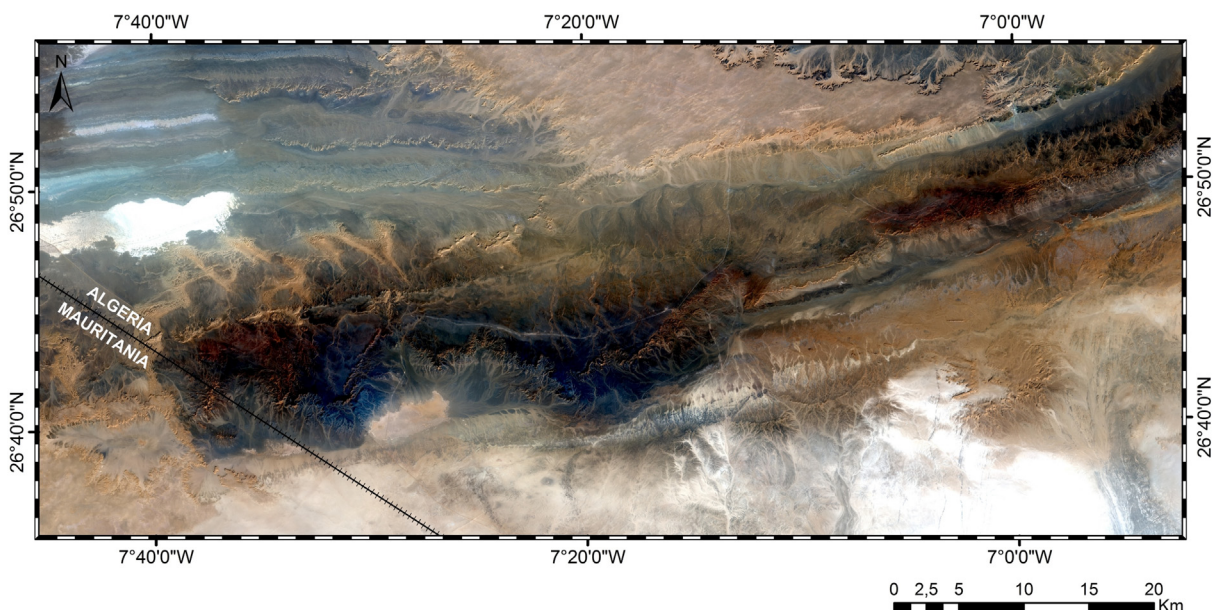


Fig. 6. Natural light composite of the Djebilet area. The OLI panchromatic band (0.50–0.68 μm) has been used to sharpen the resolution of the red, green and blue bands. (For interpretation of the references to color in this figure legend, the reader is referred to the web version of this article.)

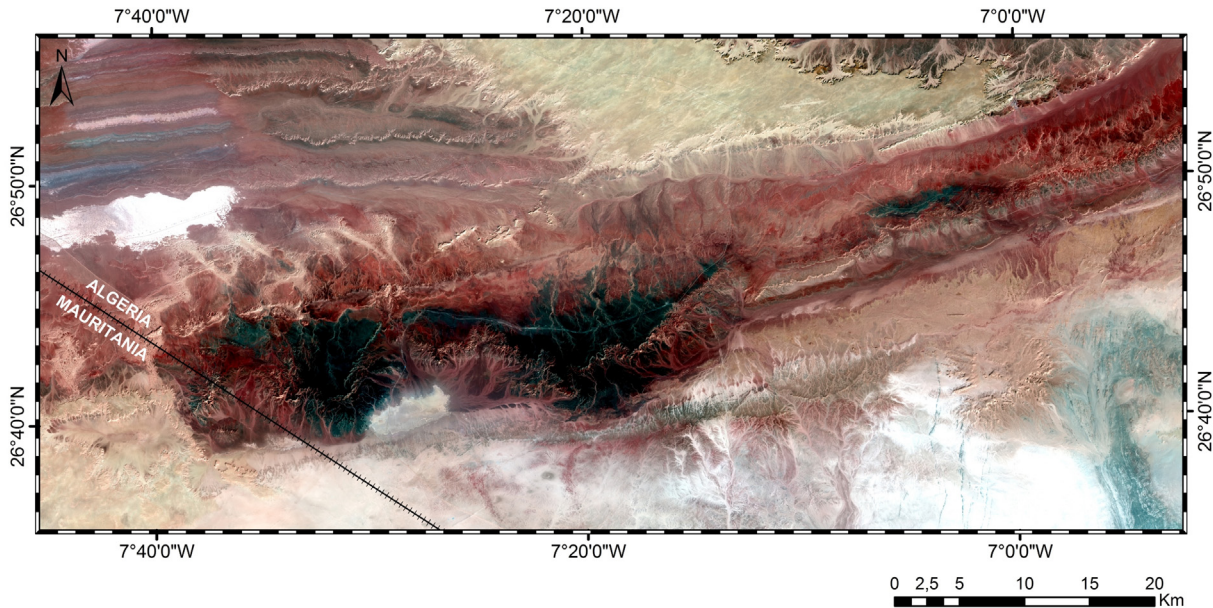


Fig. 7. False color composite using bands 6, 5 and 4 displayed in RGB mode, respectively. The iron ore corresponds to the deep blue zone. (For interpretation of the references to color in this figure legend, the reader is referred to the web version of this article.)

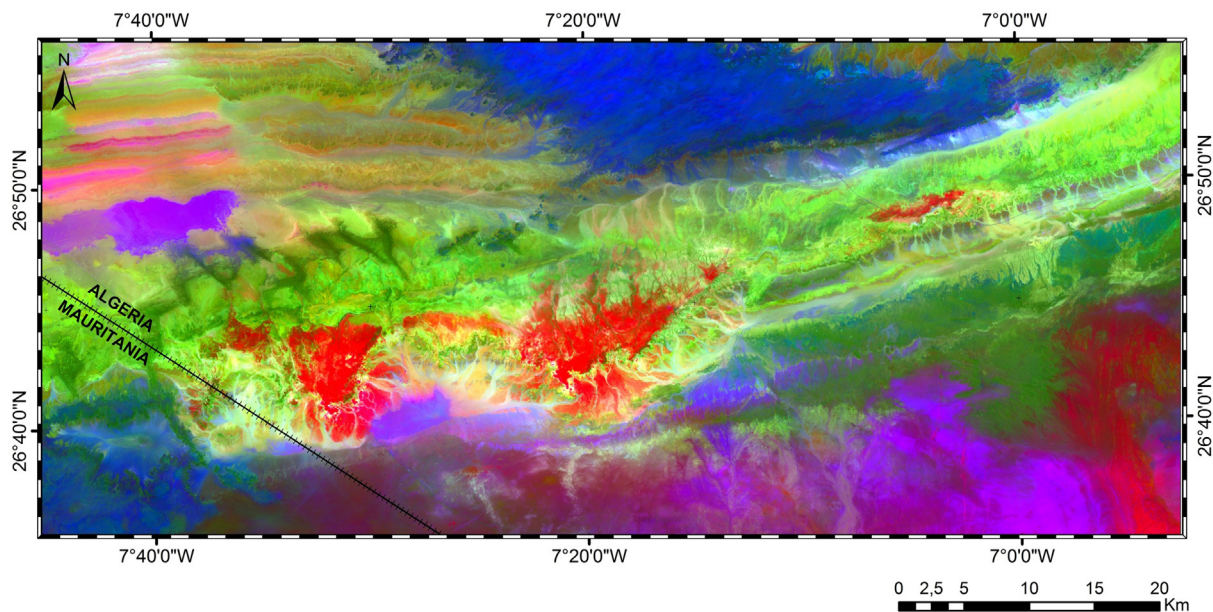


Fig. 8. OLI band ratios 4/5, 5/6 and 6/7 displayed, respectively, in RGB mode. The reddish zone corresponds to the high iron content.

while the other formations present values less than 1. The iron ore is highlighted with a red color.

The same ratios are pan-sharpened using panchromatic bands; the new ratios are displayed in RGB mode. The iron ore is well highlighted with a deep green color (Fig. 10); geologic features and the hydrographic network are best observable in this image with a 15-m resolution.

4.3. Principal component analysis (PCA)

PCA can be useful for reducing data redundancy, suppressing data noise, or enhancing particular patterns. Most of the variability

in the original variables is detected in the first few PC (Yang, 2009). PCA imagery is very useful in geological recognition. The covariance matrix is used in this transformation. The 6 multispectral bands are used (2–7); correlation coefficients are displayed in a radar plot (see Fig. 5), and this figure shows that the fourth component (PC4) is the most correlated with the other components. Ciampalini et al. (2013a,b) revealed that PC4 usually contains spectral/lithological information; this component is used to display in rainbow colors using the ENVI color table (Fig. 11). In this figure, we can distinguish three levels of iron content, with the first one in red corresponding to high iron content, the second level in orange corresponding to medium iron content and the last one in yellow corresponding to

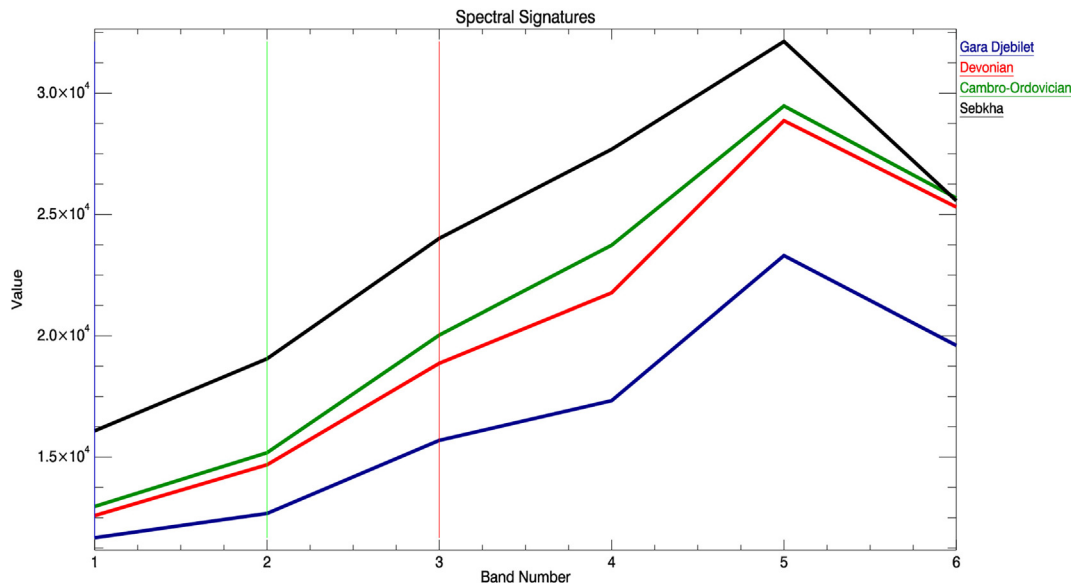


Fig. 9. Spectral signature of the Gara Djebilet deposit and surrounding formations.

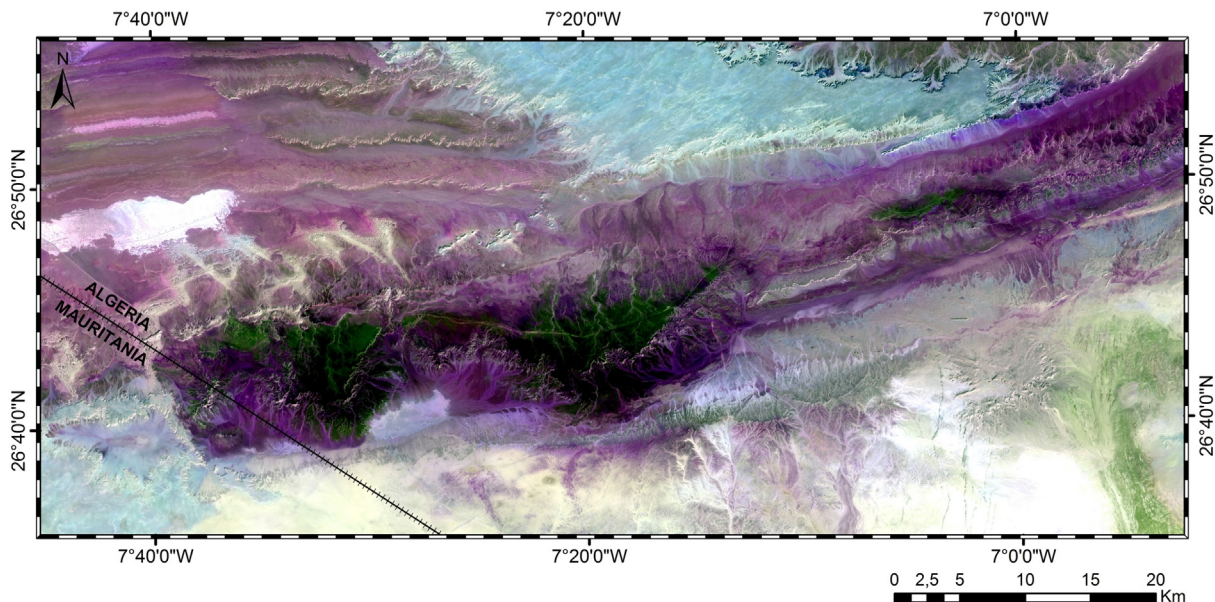


Fig. 10. OLI pan-sharpened ratios 4/5, 5/6 and 6/7 displayed, respectively, in RGB mode. The high iron content corresponds to the deep green zone. (For interpretation of the references to color in this figure legend, the reader is referred to the web version of this article.)

low iron content. PC4, PC3 and PC2 displayed in RGB mode, respectively (Fig. 12), proved the best composite to highlight iron ore; the iron formations are in white, and boundaries are well observable.

4.4. Iron ore index

Indexes are mathematical operations applied to bands on satellite images. Operations include addition, subtraction and division. Indices have recently proved most useful in geological and environmental studies. Hassani et al. (2015) performed the index of water surfaces (IWS) using Landsat 7 ETM+ images. The main objective of the iron ore index is to make iron mapping easier. The index consists of applying mathematical equation (1) to a Landsat 8

image. The first step is to visualize the spectral behavior of iron ore formations and nearby formations and classify radiometric intervals for each formation. The second step is to find specific radiometric intervals for the iron ore, in this area usually corresponding to absorption bands in the range of 0.88–2.27 μm . The intervals where the iron ore and surrounding formations have the same spectral behaviors are not used to perform the iron ore index. We note that in the visible range, the Sebkhas and Reguibat formations have high reflectance values, which cause confusion with the iron ore formations when dividing; therefore, only the near infrared channels were used. The final step consists of choosing the optimum combination of these three bands (bands 5, 6 and 7). The iron ore absorbs electromagnetic radiation in band 5 (Escadafal, 1994; Mathieu et al., 1998; Ciampalini, 2013a, b; Pirie et al., 2005)

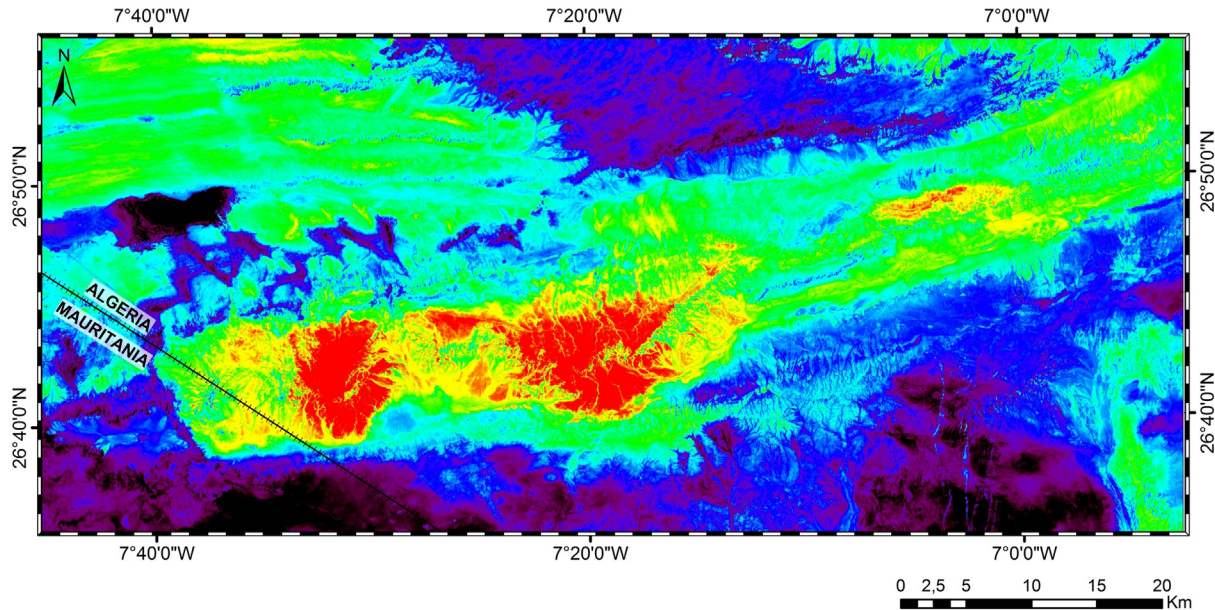


Fig. 11. PC4 displayed in rainbow colors using the ENVI color table. In this figure, we can distinguish three levels of iron content: the first level in red, corresponding to high iron content; the second level in orange, corresponding to medium iron content; and the last level in yellow, corresponding to low iron content. (For interpretation of the references to color in this figure legend, the reader is referred to the web version of this article.)

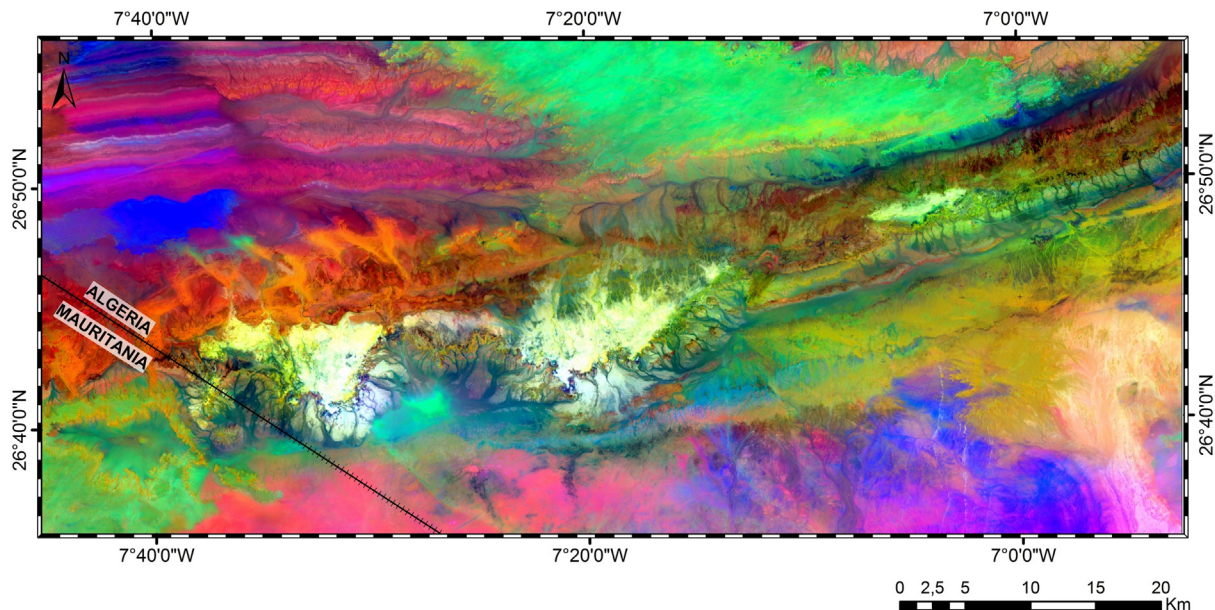


Fig. 12. PC4, PC3 and PC2 displayed in RGB mode, respectively. The white zone corresponds to the iron deposit.

and absorbs less in bands 6 and 7. The Paleozoic formations absorb electromagnetic radiation in band 7 due to clay mineral enrichment. Dividing band 6 by band 5 shows the iron ore in a dark color and the other formations in gray shades. Multiplying band 6 by 2 increases the range between iron ore values in bands 6 (B6) and 5 (B5), and the iron ore will present low values displayed as a black color in this new channel. The iron ore in this new channel is not the only formation displayed in black as the Sebkha and Reguibat formations are also in black. To solve this, we must subtract their formations by applying some additional operations. The Sebkha and Reguibat formations are well highlighted by dividing band 5 by

band 7 (B7), and when multiplying the numerator by 3, these formations will appear in black. The last operation consists of subtracting $3 \times B5/B7$ from $2 \times B6/B5$. The final result (Fig. 13) shows the iron ore in black and all other formations in white, and a simple vectorization of the obtained raster image gives us the shape of the iron ore, and the perimeter and area are easily obtained from GIS software.

The application of mathematical operations to the bands allows the creation of neo-channels with the objective of highlighting the iron ore. Addition, subtraction and division have been used to define the iron ore index as follows:

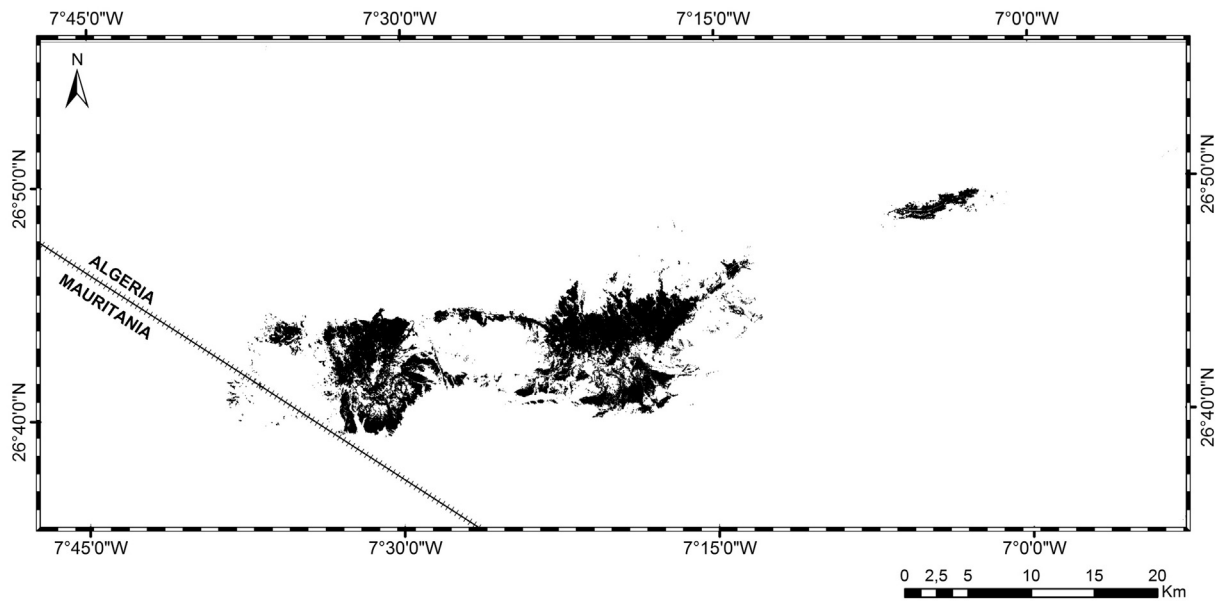


Fig. 13. Iron ore index. The iron ore is in black, and all other formations are in white.

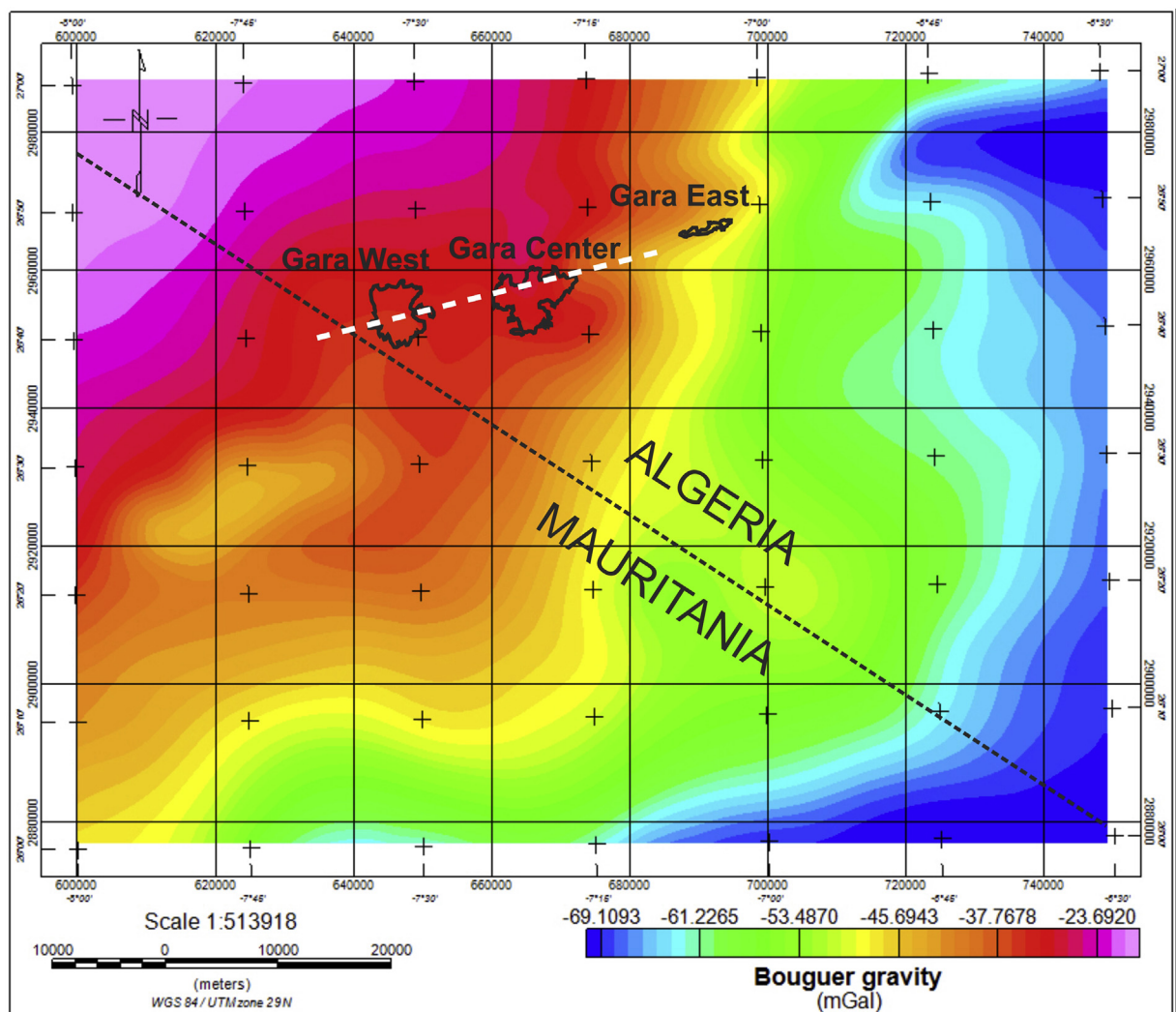


Fig. 14. Bouguer gravity anomaly map (mGal) of the study area with the location of the profile for 2-D forward gravity modeling in white-dashed line.

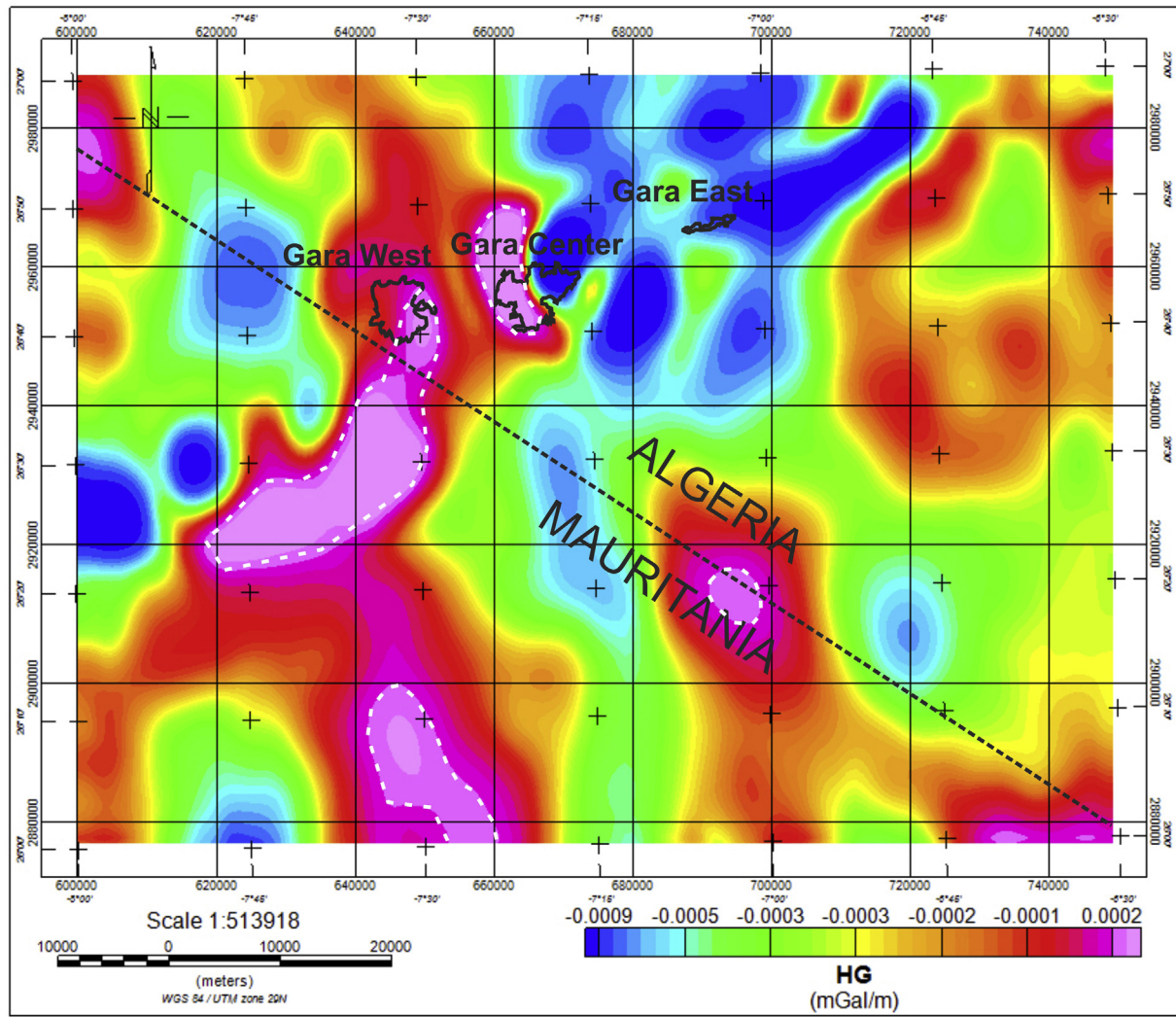


Fig. 15. Horizontal gradient map of gravity data. White dashed line indicates the limits of the high HG values interpreted as high-density rocks.

$$\text{Iron ore index} \rightarrow \left[\frac{2 \times B6}{B5} - \frac{3 \times B5}{B7} \right] \quad (1)$$

5. Gravity data analysis

The gravity dataset is composed of 864 gravity measurements and is derived from the Earth Geopotential Model EGM2008 provided by the National Geospatial Intelligence Agency (Bonvalot et al., 2012). The data were already corrected for elevation and topographic effects, and a Bouguer density of 2.67 g/cm^3 was used to calculate the Bouguer gravity. The Bouguer gravity data range between -69 and -20 mGal (Fig. 14). The grid size of the data is 100 m and the line spacing is 4 km .

In general, the Bouguer gravity increases from SE to NW. The high Bouguer gravity in the NW of Gara Djebilet is due to the uplift of basement rocks in southern of Tindouf Basin.

A very high local anomaly is observed at Gara Center, and high anomalies are seen at Gara West and Gara East (Fig. 14). The local high Bouguer gravity anomalies explain the high density underground just below the anomalies.

Many gravity data interpretation methods have been developed

over the last three decades to determine the location of gravity sources, which helps in geological interpretation. The gravity interpretation methods we use here are: Horizontal Gradient (HG), Analytic Signal (AS), and Tilt Derivative (TDR). The different derivative methods were applied after upward continuation of the gridded Bouguer gravity data by 2000 m to avoid artifacts.

A 3-D inversion of gravity data was also performed to show the underground density distributions in the study area.

5.1. Horizontal gradient

The HG method has a characteristic to locate density contrast boundaries from gravity data (Grauch and Cordell, 1987; Fedi and Florio, 2001) and can delineate shallow and deep gravity sources. Maxima in the HG indicate the location of faults or contacts. The equation of the HG (Cordell and Grauch, 1985) is given as:

$$\text{HG} = \sqrt{\left(\frac{\partial g}{\partial x} \right)^2 + \left(\frac{\partial g}{\partial y} \right)^2}, \quad (2)$$

where g is the gravity field observed at (x, y) , and $\partial g/\partial x$ and $\partial g/\partial y$ are the two horizontal derivatives of the gravity field in the x- and y-directions. The results of the HG of gravity data for Gara Djebilet

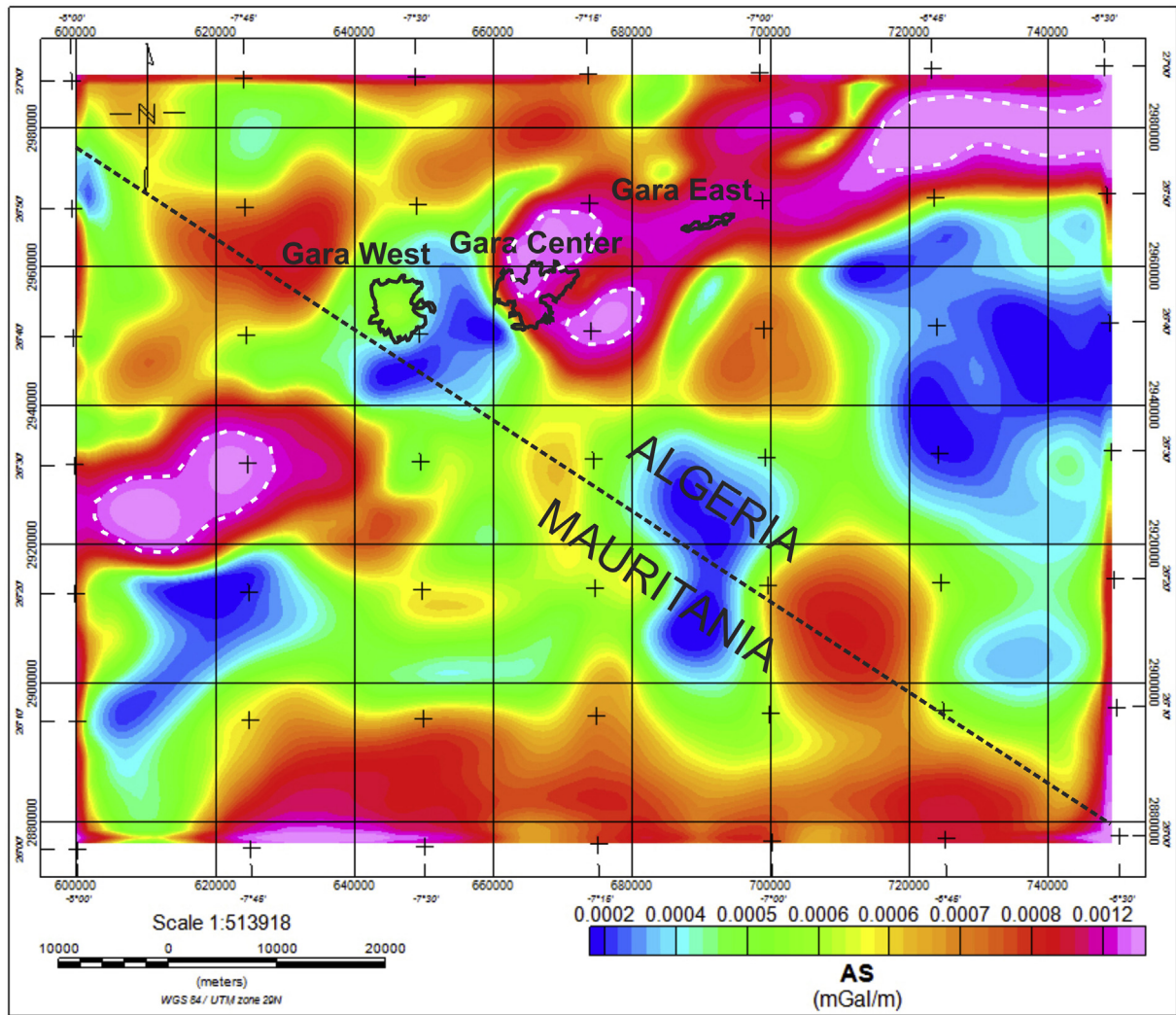


Fig. 16. Analytic signal map of gravity data. White dashed line shows the limits of the high AS values explained as high-density rocks.

are shown in Fig. 15.

High HG anomalies are observed over the location of iron ore deposits, especially at Gara west and western part of Gara center. A high gradient features with gravity exceeding 0.2 mGal/km trends NE-SW. Two other high anomalies are also observed in south and south-east of Gara Djebilet.

5.2. Analytic signal

The AS method (Nabighian, 1972) has been the subject of continuing investigation and improvements since it was first applied (e.g., Nabighian, 1974, 1984; Roest et al., 1992; MacLeod et al., 1993; Hsu et al., 1996, 1998; Debeglia and Corpel, 1997; Keating and Pilkington, 2004; Saibi et al., 2006). The AS peaks over the location of the top of the contact or fault. The general equation for a 3D gravity source (Klingele et al., 1991) is:

$$|AS(x, y)| = \sqrt{\left(\frac{\partial g}{\partial x}\right)^2 + \left(\frac{\partial g}{\partial y}\right)^2 + \left(\frac{\partial g}{\partial z}\right)^2} \quad (3)$$

where $|AS(x, y)|$ is the amplitude of the analytic signal at (x, y) , g is the gravity field observed at (x, y) , and $\frac{\partial g}{\partial z}$ is the vertical derivative of the gravity field.

The AS map shows clear maximum AS values (higher than 1.2 mGal/km) over the causative iron ore bodies especially at Gara center and Gara east (Fig. 16). The high AS values are trending WSW-ENE, which correlates with the results of HG.

5.3. Tilt derivative

The TDR method was applied to enhance the potential field anomalies. The zero value of the TDR delineates the source edges. The TDR (Miller and Singh, 1994) is described as (Fig. 17):

$$TDR = \tan^{-1} \left\{ \frac{\frac{\partial g}{\partial z}}{\sqrt{(\frac{\partial g}{\partial x})^2 + (\frac{\partial g}{\partial y})^2}} \right\} \quad (4)$$

5.4. Forward and inverse modeling

5.4.1. 2-D forward modeling

A 2-D forward-gravity model (Fig. 18) was constructed along a profile (see Fig. 14) using the GM-SYS program (GM-SYS User's Guide, 2004), based on the algorithms developed by Rasmussen

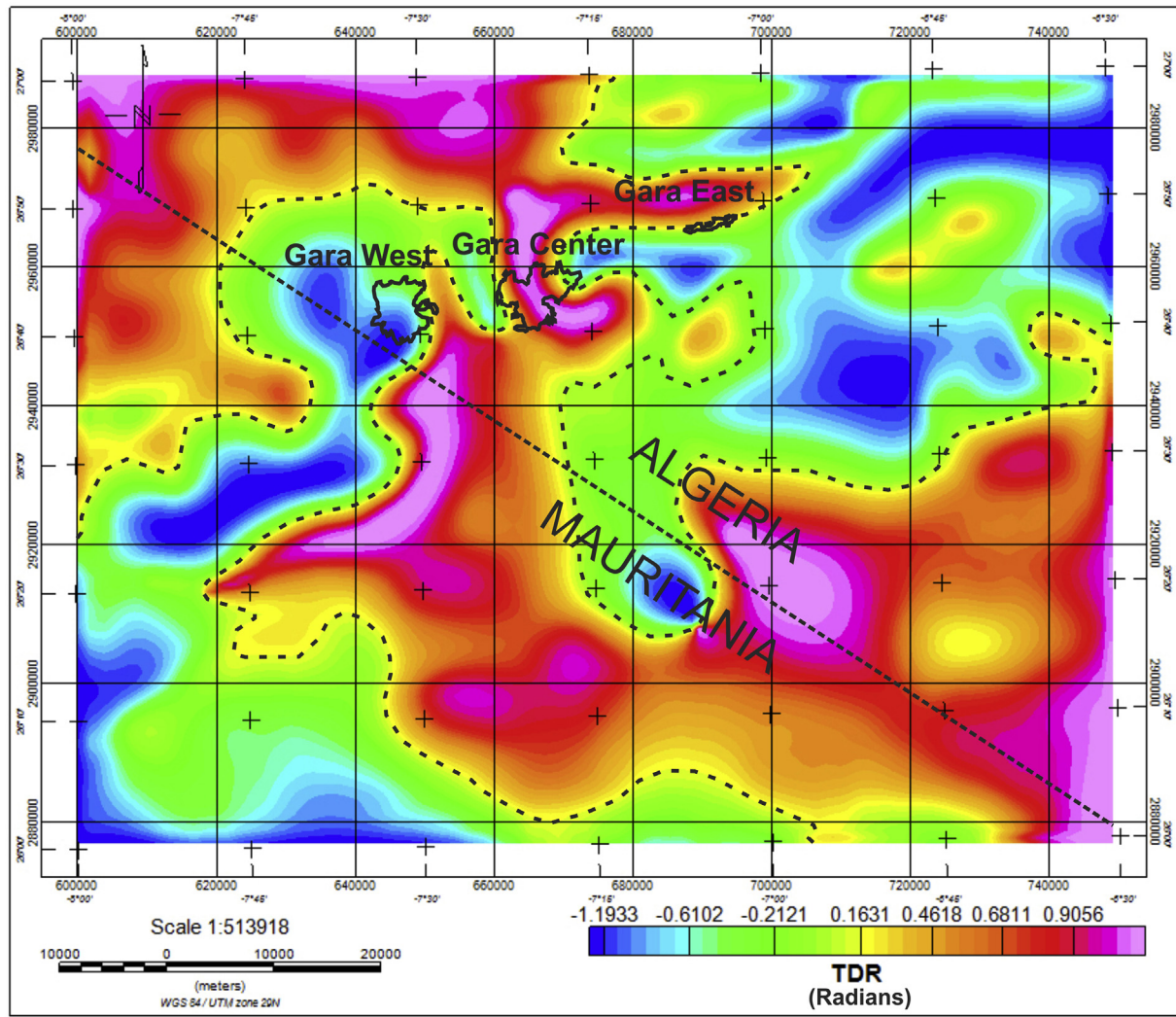


Fig. 17. Tilt derivative of gravity data. The black dashed line shows the zero-value TDR.

and Pedersen (1979) and Won and Bevis (1987). GM-SYS allows forward modeling of the gravity data to obtain the best matching between the calculated and observed gravity data.

To compute the 2-D gravity model, the subsurface geological layers were assumed to be five polygons based on the lithological characteristics of the study area, and then density values were assigned to each geological layer. The gravity field response is calculated and visually compared with the measured data. We assumed an average density for the iron ore of 3.5 g/cm^3 based on the average density of common rock-forming and ore minerals (Dentith and Mudge, 2014).

The topography was also taken into account during the modeling process. A good match (best fit) was achieved between observed and calculated gravity data, and the result is shown in Fig. 18.

5.4.2. 3-D gravity inversion

Potential-field inversions are commonly used for mineral and structural investigations. Martinez et al. (2013) successfully inverted the airborne gravity gradiometry data to delineate the iron ore formation in Quadrilatero Ferrifero (Brazil).

The forward modeling of gravity data is adequate for testing the gravity response for different structures and geometries; however,

the 3-D gravity approach is much sophisticated and the response can be checked and modified until a good agreement with measured gravity field is achieved.

A 3-D inversion model of the aerogravity data from the Gara Djebilet region was developed using VOXI earth modeling tool in Geosoft Oasis Montaj Ver. 8.4 (Fig. 19 A). The model covers $16,650 \text{ km}^2$ (150 km in the x-direction and 111 km in the y-direction) with 50 grid-blocks in the x-direction and 37 grid-blocks in y-direction. Vertically, the model extends from the Earth's surface to 11,695 m below the surface, discretized using 23 grid-blocks. The horizontal and vertical increment is constant for all cells above the lowest point of the terrain. Below that level, the cell size increases by the given cell expansion ratios shown in Table 2.

As is customary, the vertical extents of the cells are allowed to gradually increase with depth, reflecting the loss of resolution. The gravity data were inverted using Geosoft VOXI smooth model inversion, and the results are summarized in Tables 1 and 2. The unconstrained density results give smooth distributions of both positive and negative density contrasts. Blocks with density contrasts of 1.5 g/cm^3 , 1.0 g/cm^3 and 0.5 g/cm^3 are shown in Fig. 19 (B, C, D), respectively.

The density contrast between the iron deposits and the surrounding rock is approximately 0.5 g/cm^3 , as modeled in the

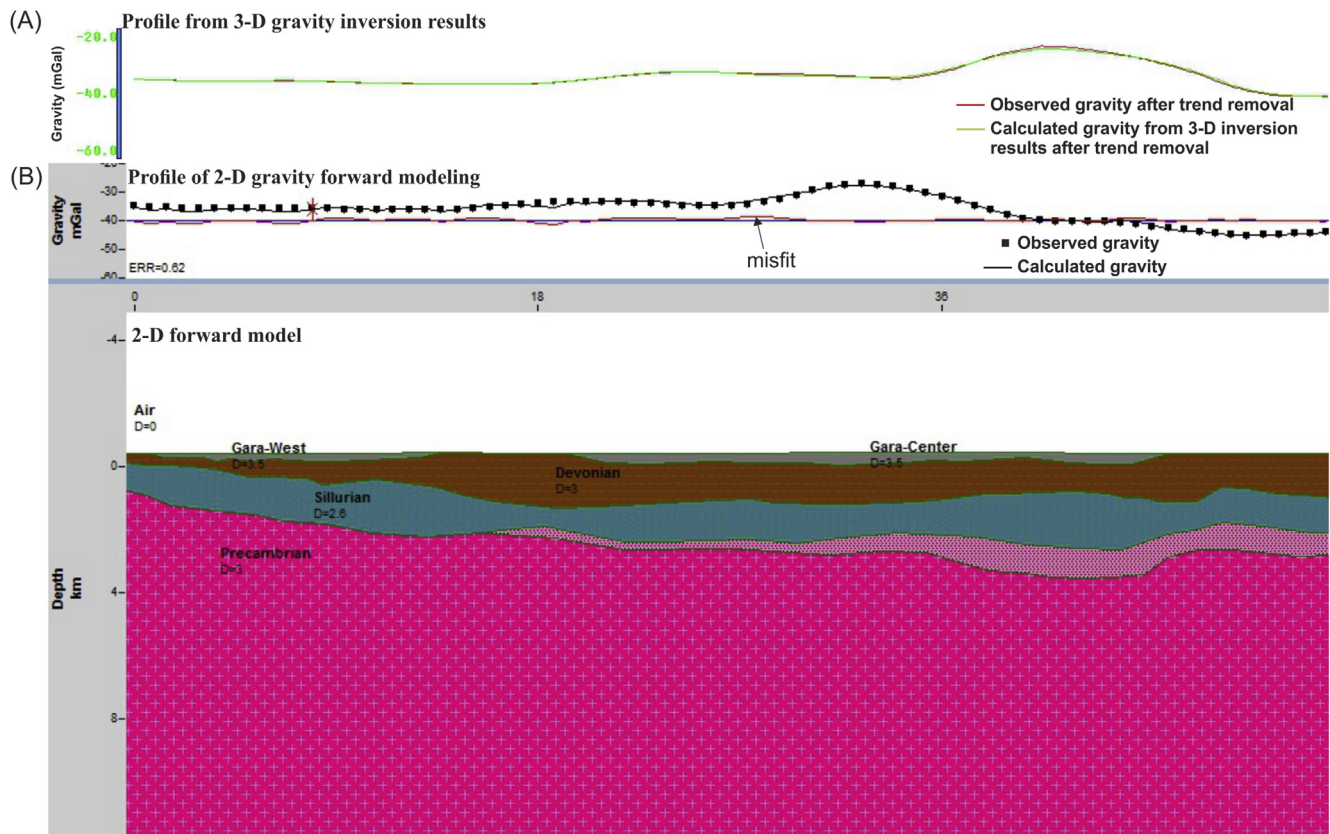


Fig. 18. 2-D forward model of gravity data along the ENE-WSW profile. (A) shows the gravity data comparison along the same 2-D forward model profile between observed gravity data and calculated gravity from 3-D inversion results. (B) shows the good correlation between the observed gravity data and the model response from 2-D forward modeling results. The differences between the results from 2-D forward modeling and 3-D inversion are due to the effects of trend removal, which is applied in the 3-D inversion calculations, and the 2-D forward modeling does not take into account the Y-direction in the calculations.

forward model (Fig. 18). In this case, the inversion results presented in Fig. 19(D) are the most probable for the location of the iron deposits. For this situation, four blocks are detected in the inversion model (Fig. 19 E). These four blocks have a total volume of 7.2 km^3 , and each block has dimensions of $3 \text{ km} \times 3 \text{ km} \times 0.2 \text{ km}$.

6. Discussion and conclusions

The Gara Djebilet iron ore is the most important iron deposit in Algeria. Because it is situated in the southwestern part of Algeria and is difficult to access, remote sensing techniques (Landsat 8 images and airborne gravity data) are integrated in this study to investigate the iron ore deposit.

In the remote sensing analysis, several treatments are applied, including color composites, bands ratioing, principal component analysis and indexing. The results obtained allowed us to map the iron ore boundaries and to obtain the surface distribution of the iron formations. The iron ore index applied to OLI multispectral images is the most efficient image processing result, allowing a fast surface detection of the extent of the iron, and the obtained raster image could be saved as an 8-bit GeoTIFF image, which can be imported to a GIS environment from which a simple vectorization area and perimeter are easily obtained. The iron ore surface manifestation occupies an area of 123.89 km^2 ; this very important area measurement confirms the importance of this deposit.

The different gravity derivative methods helped us to map the extension of iron deposits and detect their limits. The limits of iron deposits exceed the outcropping iron regions and can not be seen on the surface due the sedimentary cover. The general trend of the

iron deposits is WSW-ENE to SW-NE, which is the same direction detected by geological and remote-sensing mapping.

The high gradient anomaly detected by HG technique observed in the south-east of Gara Djebilet ($26^{\circ}20'N$ $7^{\circ}05'W$) is explained by the intrusion of an ultramafic body (the Gara Djebilet ring structure), interpreted as an outcrop from a huge subsurface magma chamber composed of ultramafic rocks (Tabeliouna et al., 2008).

Another high gradient anomaly detected by AS technique observed in the north-east of Gara Djebilet ($26^{\circ}50'N$ - $27^{\circ}00'N$, $6^{\circ}30'W$ - $6^{\circ}55'W$) and located above the paleozoic cover of the Tindouf basin where doleritic sills of the CAMP are abundant (Gevin, 1960; Chabou et al., 2010). These dense dolerites may also explain these anomalies.

Finally, the NE-SW trending high anomalies in Mauritania may be the continuity of the iron deposits because in the Mineral map of Mauritania, it is reported an iron deposits near the Algerian border (MPEM-IRM, 2015).

A good agreement was observed between the location of the causative bodies detected by gravity gradient interpretation techniques and the results of remote sensing.

Analysis of gravity data could estimate the iron reserve geophysically based on geological and remote sensing assumptions. The calculated tonnages using information from remote sensing data and geophysical results are presented in Table 3.

The density of iron ore is assumed to be 3.5 g/cm^3 . We used the results of the remote sensing image analyses for an area extent of 123.89 km^2 . For the thickness of the iron ore bodies, two values were selected, one of 30 m from geological information and the other of approximately 100 m from the gravity forward model,

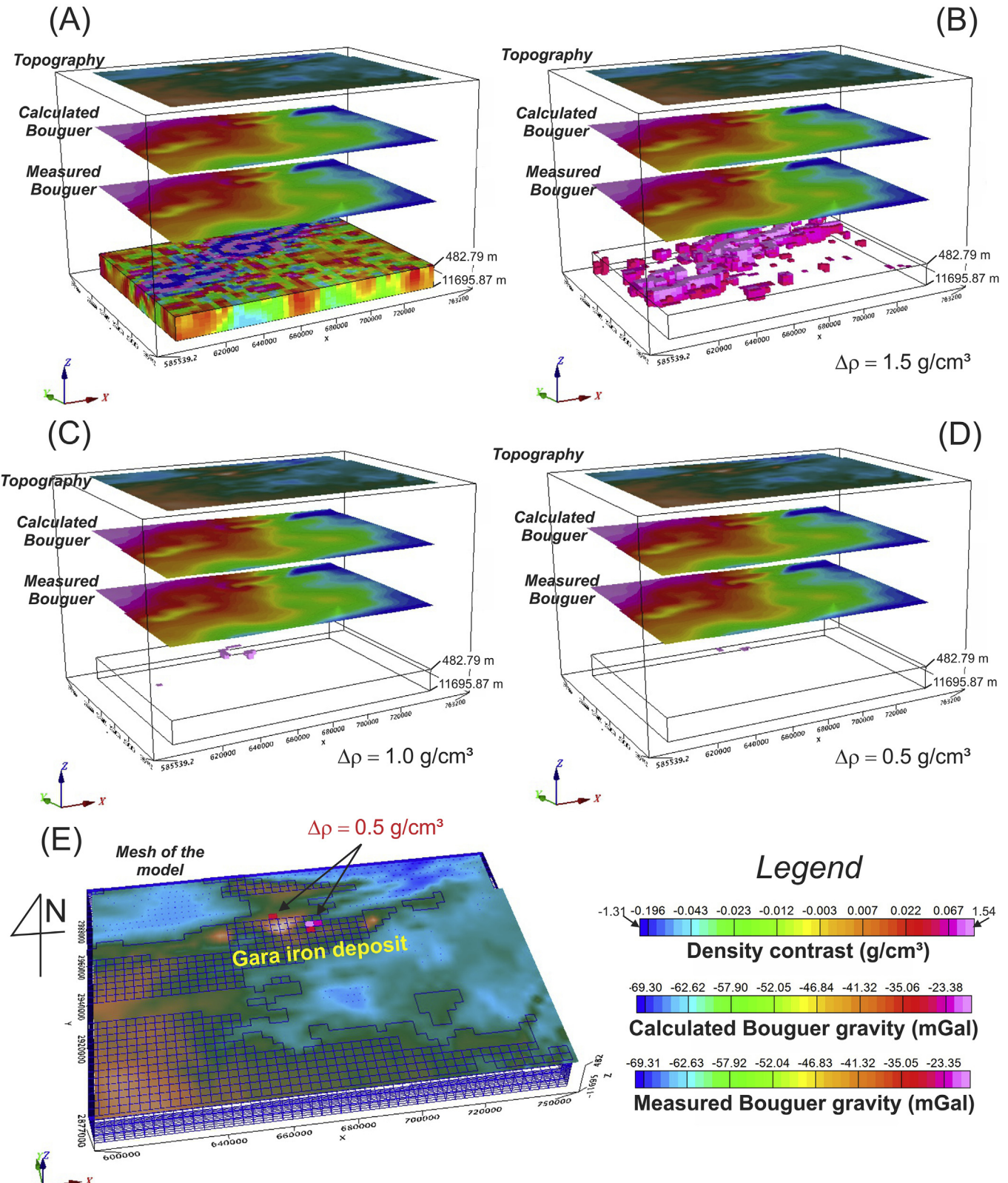


Fig. 19. (A) Results of 3-D gravity data inversion from Gara Djebilet, (B) Blocks with a density contrast of 1.5 g/cm^3 , (C) Blocks with a density contrast of 1.0 g/cm^3 , (D) Blocks with a density contrast of 0.5 g/cm^3 , (E) Mesh of the model showing the location of blocks with a density contrast of 0.5 g/cm^3 .

Table 1
Mesh parameters of the active volume of the gravity data.

	X	Y	Z
Cell size (m)	3000	3000	200
Dimensions (cells)	50	37	23
Minima (m)	600630.0	2878607.6	-10845.0
Maxima (m)	747163.9	2986960.1	482.8

Table 2
Mesh parameters of the base and padding of the gravity data.

	Base	Horizontal padding	Vertical padding
Dimensions (cells)	22	5	5
Cell expansion ratios	1.08	1.5	1.5

Table 3

Estimation of ore tonnage in Gara Djebilet.

Parameters	Approach			
	Geology	2-D forward gravity modeling	3-D gravity inversion	Remote sensing images
Surface area (A)	—	—	36 km ²	123.89 km ²
Thickness (H)	30 m	100 m	200 m	—
Volume (V)	3.72 km ³ (using A = 123.89 km ²)	24.78 km ³ (using A = 123.89 km ²)	7.2 km ³ (4 blocks × 3000 m × 3000 m × 200 m)	—
V = A × H	—	—	—	—
Mass (M) = ρ × V	1.3 × 10 ¹³ kg	4.33 × 10 ¹³ kg	2.52 × 10 ¹³ kg	—
(ρ = 3.5 g/cm ³)	—	—	—	—
Tonnage (T) at 57% Fe	7.41 × 10 ⁹ T	27.20 × 10 ⁹ T	15.83 × 10 ⁹ T	—

(-) No data.

giving tonnages of 7.4 billion tonnes and 27.2 billion tonnes, respectively, at a 57% grade. The calculated tonnage from the 3-D gravity inversion results is approximately 15.8 billion tonnes, much higher than the geological results. If we re-calculate this later tonnage (15.8 billion tonnes) for the 30 m thickness (geologically estimated thickness), the tonnage of iron deposit is 2.37 billion tonnes at a 57% grade, which is much closer to the estimated tonnage by Matheron (1955) of 2.7 billion tonnes at the same grade of Fe.

The results of this work estimate the tonnage of iron ore at approximately 2.37 billion tonnes, which is the first estimation from available airborne gravity data and satellite images and not far from previous results.

We recommend drilling projects in the study area to determine the exact thickness of the iron ore strata and its vertical extent to create a new inversion model with a priori information and geological constraints for better iron ore tonnage estimation. We recommend rock density measurements that will help us in the gravity modeling. We also recommend full tensor airborne gravity gradiometry for better estimation of total anomalous mass as applied by Braga et al. (2014) in exploring iron ore deposits in Minas Gerais (Brazil) and an aeromagnetic survey, which will mainly help locate the magnetite in this area.

Acknowledgments

The authors are grateful to the Editor Dr. R.B.M. Mapeo and two anonymous referees for their comments and suggestions to improve this paper.

References

- Abulghasem, Y.A., Akhir, J.M., Samsudin, A.R., Hassan, W.F.W., Youshah, B.M., 2011. Integrated data of remote sensing and geophysical data for iron ore exploration in the western part of Wadi Shatt District, Libya. *EJGE* 16, 1441–1454.
- Bitam, L., Gourvennec, R., Robardet, M., 1996. Les formations paléozoïques antécarbonifères du sous-bassin de Djebilet (flanc sud du Bassin de Tindouf, Nord-Ouest du Sahara algérien). In: Bitam, L., Fabre, et J. (Eds.), *Géodynamique du craton ouest africain central et oriental: héritage et évolution post-panafricains*, 8. Mémoires du Service Géologique de l'Algérie, Boumerdès, pp. 15–22.
- Bonvalot, S., Balmino, G., Briais, A., Kuhn, M., Peyrefitte, A., Vales, N., et al., 2012. World Gravity Map. Bureau Gravimétrique International (BGI), map, Paris. CGMW-BGI-CNRS-IRD Ed.
- Braga, M.A., Endo, I., Galbiatti, H.F., Carlos, D.U., 2014. 3D full tensor gradiometry and Falcon Systems data analysis for iron ore exploration: Baú Mine, Quadrilátero Ferrífero, Minas Gerais, Brazil. *Geophysics* 79 (5), B213–B220. <http://dx.doi.org/10.1190/geo2014-0104.1>.
- Chabou, M.C., Bertrand, H., Sebai, A., 2010. Geochemistry of the Central Atlantic Magmatic Province (CAMP) in south-western Algeria. *J. Afr. Earth Sci.* 58, 211–219.
- Chabou, M.C., Sebaï, A., Feraud, G., Bertrand, H., 2007. Datation ⁴⁰Ar/³⁹Ar de la Province Magmatique de l'Atlantique Central dans le Sud-Ouest algérien. *Comptes Rendus Geosci.* 339, 970–978.
- Ciampalini, A., Garfagnoli, F., Antonielli, B., Moretti, S., Righini, G., 2013a. Remote sensing techniques using Landsat ETM plus applied to the detection of iron ore deposits in Western Africa. *Arab. J. Geosci.* 6, 4529–4546.
- Ciampalini, A., Garfagnoli, F., Ventisette, C., Moretti, S., 2013b. Potential use of remote sensing techniques for exploration of iron deposits in Western Sahara and Southwest of Algeria. *Nat. Resour. Res.* 22 (3), 179–190.
- Clénet, H., Ceuleneer, G., Pinet, P., Abily, B., Daydou, Y., Harris, E., Dantas, C., 2010. Thick sections of layered ultramafic cumulates in the Oman ophiolite revealed by an airborne hyperspectral survey: petrogenesis and relationship to mantle diapirism. *Lithos* 114 (3–4), 265–281. <http://dx.doi.org/10.1016/j.lithos.2009.09.002>.
- Cordell, L., Grauch, V.J.S., 1985. Mapping basement magnetization zones from aeromagnetic data in the San Juan Basin, New Mexico. In: Hinz, W.J. (Ed.), *The Utility of Regional Gravity and Magnetic Anomaly Maps*, Soc. Explor. Geophys., pp. 181–197.
- Debeglia, N., Corpel, J., 1997. Automatic 3-D interpretation of potential field data using analytic signal derivatives. *Geophysics* 62, 87–96.
- Dentith, M., Mudge, S.T., 2014. *Geophysics for the Mineral Exploration Geoscientist*. Cambridge University Press, p. 438.
- Dronova, I., Gong, P., Wang, L., Zhong, L., 2015. Mapping dynamic cover types in a large seasonally flooded wetland using extended principal component analysis and object-based classification. *Remote Sens. Environ.* 158, 193–206. <http://dx.doi.org/10.1016/j.rse.2014.10.027>.
- Dufrechou, G., Harris, L.B., Corriveau, L., Antonoff, V., 2015. Regional and local controls on mineralization and pluton emplacement in the Body gneiss complex, Grenville Province, Canada interpreted from aeromagnetic and gravity data. *J. Appl. Geophys.* 116, 192–205.
- Escadafal, R., 1994. Soil spectral properties and their relationships with environmental parameters-examples from arid regions. In: Hill, J., Mégier, J. (Eds.), *Imaging Spectrometry—a Tool for Environmental Observations*, pp. 71–87.
- Fabre, J., 2005. *Géologie du Sahara occidental et central*. Musée Royal de l'Afrique Centrale, p. 572.
- Fabre, J., 1976. Introduction à la géologie du Sahara algérien. SNED, Alger, p. 422.
- Fedi, M., Florio, G., 2001. Detection of potential fields source boundaries by enhanced horizontal derivative method. *Geophys. Prospect.* 49, 40–58.
- Feizi, F., Mansouri, E., 2013. Introducing the iron potential zones using remote sensing studies in South of Qom Province, Iran. *Open J. Geol.* 3, 278–286.
- Gevin, P., 1960. Études et reconnaissances géologiques sur l'axe cristallin Yetti-Eglab et ses bordures sédimentaires. Première partie. Bordures sédimentaires. *Publ. Serv. Carte Géol. Algérie*, Bull. N. S. 23, 328.
- Gevin, P., Mongereau, N., 1968. Précisions sur l'âge des grès "cambro-ordoviciens" d'Aouinet Legraa (région de Tindouf, Sahara occidental). *C. R. Somm. Soc. Géol. Fr.* 263–264.
- GMsys, 2004. *Gravity/Magnetic Modeling Software User's Guide*, Version 4.9. Northwest Geophysical Associates, Corvallis Oregon.
- Grauch, V.S.J., Cordell, L., 1987. Limitations of determining density or magnetic boundaries from the horizontal gradient of gravity or pseudogravity data. *Short note. Geophysics* 52 (1), 118–121.
- Guerrak, S., 1988. Geology of the early Devonian oolitic iron ore of the Gara Djebilet field, Saharan Platform, Algeria. *Ore Geol. Rev.* 3 (4), 333–358.
- Guerrak, S., 1991. The Palaeozoic Oolitic Ironstone Belt of North Africa: from the Zemmour to Libya. In: Salem, M.J., Busrewil, M.T., Ben Ashour, A.M. (Eds.), *The Geology of Libya*, VII. Elsevier London, pp. 2703–2722.
- Guerrak, S., Chauvel, J.J., 1985. Les mineralisations ferrifères du Sahara Algérien. Le gisement de fer oolithique de Mecheri Abdelaziz (bassin de Tindouf). *Mineral. Deposita* 20, 249–259.
- Hammer, S., 1945. Estimating ore masses in gravity prospecting. *Geophysics* 10 (1), 51–62.
- Hassani, M., Chabou, M., Hamoudi, M., Guettouche, M., 2015. Index of extraction of water surfaces from Landsat 7 ETM+ images. *Arab. J. Geosci.* 8 (6), 3381–3389.
- Hsu, S.-K., Coppens, D., Shyu, C.-T., 1998. Depth to magnetic source using the generalized analytic signal. *Geophysics* 63, 1947–1957.
- Hsu, S.-K., Sibuet, J.-C., Shyu, C.-T., 1996. High resolution detection of geologic boundaries from potential field anomalies: an enhanced analytic signal technique. *Geophysics* 61, 373–386.
- Keating, P., Pilkington, M., 2004. Euler deconvolution of the analytic signal and its application to magnetic interpretation. *Geophys. Prosp.* 52, 165–182.
- Klingele, E.E., Marson, I., Kahle, H.G., 1991. Automatic interpretation of gravity gradiometric data in two dimensions: vertical gradient. *Geophys. Prospect.* 39, 407–434.
- MPEM-IRM (Ministry of Petroleum, Energy and Mines, Islamic Republic of

- Mauritania), 2015. Accessed in 2015 at: www.mauripem.com.
- MacLeod, I.N., Jones, K., Dai, T.F., 1993. 3-D analytic signal in the interpretation of total magnetic field data at low magnetic latitudes. *Explor. Geophys.* 24, 679–688.
- Marelle, A., Abdulla, M.A., 1970. Iron ore deposits of Africa. In: Survey of World Iron Ore Resources. United Nations Dept. Econ. and Social Affairs, New York, pp. 62–101.
- Martinez, C., Li, Y., Krahenbuhl, R., Braga, M.A., 2013. 3D inversion of airborne gravity gradiometry data in mineral exploration: a case study in the Quadrilatero Ferrifero, Brazil. *Geophysics* 78 (1), B1–B11. <http://dx.doi.org/10.1190/GEO2012-0106.1>.
- Matheron, G., 1955. Le gisement de fer de Gara Djebilet. *Bulletin des Sciences Economiques BRMA*, Algérie 12, 53–63.
- Mathieu, R., Pouget, M., Cervelle, B., Escadafal, R., 1998. Relationships between satellite-based radiometric indices simulated using laboratory reflectance data and typic soil color of an arid environment. *Remote Sens. Environ.* 66 (1), 17–28.
- Miller, H.G., Singh, V., 1994. Potential field tilt – a new concept for location potential field sources. *Appl. Geophys.* 32, 213–217.
- Mouton, C.J., 2002. The use of remote sensing in iron ore exploration in the northern Cape Province of the Republic of South Africa. In: Proceedings of the International Symposium; 29th, Remote Sensing of Environment; Information for Sustainability and Development; 2002; Buenos Aires, pp. 221–225.
- Murthy, Y.V.S., Mallick, K., 1984. Interpretation of Landsat MSS data in an iron-ore-bearing zone in GOA, India. *Geophys. Prospect.* 32, 282–291.
- Nabighian, M.N., 1972. The analytic signal of two-dimensional magnetic bodies with polygonal cross-section: its properties and use for automated anomaly interpretation. *Geophysics* 37, 507–517.
- Nabighian, M.N., 1974. Additional comments on the analytic signal of two dimensional magnetic bodies with polygonal cross-section. *Geophysics* 39, 85–92.
- Nabighian, M.N., 1984. Toward a three-dimensional automatic interpretation of potential field data via generalized Hilbert transforms: fundamental relations. *Geophysics* 49, 780–786.
- Peucat, J.J., Capdevila, R., Drareni, A., Mahdjoub, Y., Kahoui, M., 2005. The Eglab massif in the West African Craton (Algeria), an original segment of the Eburnean orogenic belt: petrology, geochemistry and geochronology. *Precambrian Res.* 136, 309–352.
- Pirie, A., Singh, B., Islam, K., 2005. Ultra-violet, visible, near-infrared, and mid-infrared diffuse reflectance spectroscopic techniques to predict several soil properties. *Soil Res.* 43 (6), 713–721.
- Porter GeoConsultancy, 2015. <http://www.portergeo.com.au/database/mineinfo.asp?mineid=mn1027>. (accessed on June 2015).
- Prost, G.L., 2014. *Remote Sensing for Geoscientists, Image Analysis and Integration*, third ed. CRC Press Taylor and Francis Group, p. 674.
- Rasmussen, R., Pedersen, L.B., 1979. End corrections in potential field modeling. *Geophys. Prospect.* 29, 749–760.
- Roest, W.R., Verhoef, J., Pilkington, M., 1992. Magnetic interpretation using 3-D analytic signal. *Geophysics* 57, 116–125.
- Roy, D.P., et al., 2014. Landsat-8: science and product vision for terrestrial global change research. *Remote Sens. Environ.* 145, 154–172. <http://dx.doi.org/10.1016/j.rse.2014.02.001>.
- Sabins, F.F., 1999. Remote sensing for mineral exploration. *Ore Geol. Rev.* 14, 157–183.
- Saibi, H., Nishijima, J., Aboud, E., Ehara, S., 2006. Integrated gradient interpretation techniques for 2D and 3D gravity data interpretation. *Earth Planets Space* 58 (7), 815–821. <http://dx.doi.org/10.1186/BF03351986>.
- Seguin, M.K., 1971. Discovery of direct-shipping iron ore by geophysical methods in the Central part of the Labrador Trough. *Geophys. Prospect.* 19 (3), 459–486.
- Tabeliouna, M., Cottin, J.-Y., Kollé, O., Zerka, M., 2008. The clinopyroxinites and associated gabbros of the ring shaped magmatic complex (south of Gara Djebilet, Eglab, Reguibat Rise, Algerian SW). *Bull. Du. Serv. Géologique Natl.* 19 (3), 245–265.
- Taib, M., 2009. The Mineral Industry of Algeria. U.S. Geological Survey, 2009. Minerals Yearbook Algeria, p. 13.
- Vogt, F., Tacke, M., 2001. Fast principal component analysis (PCA) of large data sets. *Chemom. Intell. Lab. Syst.* 59, 1–18.
- Vrabel, J., 1996. Multispectral imagery band sharpening study. *Photogrammetric Eng. Remote Sens.* 62, 1075–1084.
- Vrabel, J., Doraiswamy, P., Stern, A., 2002. In: Application of Hyperspectral Imagery Resolution Improvement for Site-specific Farming, ASPRS 2002 Conference Proceedings.
- Wang, G., Zhu, Y., Zhang, S., Yan, C., Song, Y., Ma, Z., Hong, D., Chen, T., 2012. 3D geological modeling based on gravitational and magnetic data inversion in the Luanchuan ore region, Henan Province, China. *J. Appl. Geophys.* 80, 1–11.
- Won, I.J., Bevis, M., 1987. Computing the gravitational and magnetic anomalies due to a polygon: algorithms and Fortran subroutines. *Geophysics* 52, 232–238.
- Woolrych, T.R.H., Christensen, A.N., McGill, D.L., Whiting, T., 2015. Geophysical methods used in the discovery of the Kitumba iron oxide copper gold deposit. *Interpretation* 3 (2), SL15–SL25. <http://dx.doi.org/10.1190/INT-2014-0201.1>.
- Yang, X., 2009. Integrating satellite imagery and geospatial technologies for coastal landscape pattern characterization. In: Yang, X. (Ed.), *Remote Sensing and Geospatial Technologies for Coastal Ecosystem Assessment and Management*. Springer Berlin Heidelberg, pp. 461–491.